

Apparent Differences between Single Layer Molybdenum Disulfide Fabricated via Chemical Vapor Deposition and Exfoliation

Erik Pollmann,^{*,†} Lukas Madauß,[†] Simon Schumacher,^{†,‡} Uttam Kumar,^{†,¶}
Flemming Heuvel,[†] Christina vom Ende,[†] Sümeyra Yilmaz,[†] Sümeyra
Gündörmüs,[†] and Marika Schleberger[†]

[†]*Faculty of Physics and CENIDE, University of Duisburg-Essen, Lotharstraße 1, 47057
Duisburg, Germany*

[‡]*present affiliation: Technical Chemistry III & Faculty of Chemistry, University of
Duisburg-Essen, Carl-Benz-Str. 199, 47057 Duisburg, Germany*

E-mail: erik.pollmann@uni-due.de

Abstract

Innovative applications based on two-dimensional solids require cost-effective fabrication processes resulting in large areas of high quality materials. Chemical vapour deposition is among the most promising methods to fulfill these requirements. However, for 2D materials prepared in this way it is generally assumed that they are of inferior quality in comparison to the exfoliated 2D materials commonly used in basic research. In this work we challenge this assumption and aim to quantify the differences in quality for the prototypical transition metal dichalcogenide MoS₂. To this end single layers of MoS₂ prepared by different techniques (exfoliation, grown by different chemical vapor deposition methods, transfer techniques, and as vertical heterostructure with

graphene) are studied by Raman and photoluminescence spectroscopy, complemented by atomic force microscopy. We demonstrate that as-prepared MoS₂, directly grown on SiO₂, differs from exfoliated MoS₂ in terms of higher photoluminescence, lower electron concentration, and increased strain. As soon as a water film is intercalated (e.g., by transfer) underneath the grown MoS₂, in particular the (opto-)electronic properties become practically identical to those of exfoliated MoS₂. A comparison of the two most common precursors shows that the growth with MoO₃ causes greater strain and/or defect density deviations than growth with ammonium heptamolybdate. As part of a heterostructure directly grown MoS₂ interacts much stronger with the substrate, and in this case an intercalated water film does not lead to the complete decoupling, which is typical for exfoliation or transfer. Our work shows that the supposedly poorer quality of grown 2D transition metal dichalcogenides is indeed a misconception.

Keywords

Chemical Vapour Deposition, MoS₂, 2D Materials, van der Waals Heterostructures, Raman Spectroscopy

Introduction

Two-dimensional (2D) materials are in general thin, flexible, and transparent and it is expected that the semiconducting ones among them will soon play an important role in the development of flexible (opto)electronics. In particular, the possibility to stack different 2D materials to design artificial solids with tailored and otherwise inaccessible (opto)electronic properties, has opened the door for a technological breakthrough. However, one of the biggest obstacles that must be overcome before any dreams of real-world application may come true is the manufacturing process: While researchers rely heavily on isolating techniques yielding individual crystallites of 2D materials, industrial implementation requires growth techniques

which are scalable, cost-effective, and reliable.

Several hundred 2D materials could be realized so far, but the transition metal dichalcogenides (TMDCs) are the most intensively studied. This is certainly due to their physical properties, such as a large band gap in the visible range, but also to the fact that they are relatively easy to produce. Like graphene, TMDC monolayers can be isolated, e.g., by mechanical exfoliation^{1,2} and can be grown, e.g., via chemical vapour deposition (CVD).³⁻⁵ Like in the case of graphene, most basic research is still done with exfoliated flakes as it is commonly believed that their quality exceeds that of CVD grown flakes. However, the term *quality* usually refers to defect densities, and it has already been shown that 2D materials grown by CVD can exhibit defect densities which are comparable to those of exfoliated material.⁶ Thus, for graphene, being metallic, the common belief could indeed be true, as any crystalline defects are detrimental for its outstanding transport properties. For the optoelectronic properties of a semiconducting 2D material, however, appropriate quality criteria might be quite different. For example, the comparison between CVD grown MoS₂ with exfoliated MoS₂, both on sapphire,⁴ or in this study on SiO₂ (see Fig. 1 below), shows a much higher photoluminescence (PL) intensity in the case of CVD growth. Not as obvious as the intensity of a PL signal, but equally important, are the changes of the Raman mode positions for MoS₂ fabricated from CVD and exfoliation, which can be directly attributed to physical properties such as strain and doping.⁷⁻¹⁵

A pertinent problem in this context is that any comparison between 2D materials from CVD and exfoliated 2D materials requires that the materials be measured under the same or at least similar environmental conditions. Otherwise, if distinct differences are revealed, they can either be attributed to the material's quality, e.g., preparation-specific inhomogeneities, but they could also originate from preparation conditions or the chosen substrate,¹⁶⁻¹⁸ as 2D materials are extremely sensitive to their immediate surroundings. For van der Waals (vdW) heterostructures this becomes even more critical as a number of interfaces are involved which may involve any combination of exfoliated and CVD grown materials. The lack of

spectroscopic data taken on differently prepared samples under the strict condition of similar environmental conditions renders it currently almost impossible to decide, how much of what has been derived from experiments on exfoliated materials, or whether any of the reported proof-of-principle concepts may be transferred to CVD grown material at all.

In this paper we fill this crucial gap and clarify the origin of apparent spectroscopic (PL, Raman) differences found for MoS₂ either grown by CVD or isolated by exfoliation. For our comprehensive study we use exfoliated MoS₂ as a reference system, grow samples via CVD using two different precursors (molybdenum trioxid (MoO₃) and ammonium heptamolybdate (AHM)) and apply transfer techniques to obtain similar environmental conditions for MoS₂ fabricated by exfoliation and by CVD, respectively. Our experimental data shows that as prepared, MoS₂ directly grown on SiO₂ differs from exfoliated MoS₂ in terms of higher photoluminescence, lower electron concentration, and increased strain, seemingly supporting the widely shared belief of supposedly superior quality of exfoliated material. However, adding intercalated water turns the picture upside-down: We provide clear evidence by Raman spectroscopy in conjunction with PL spectroscopy and atomic force microscopy (AFM) that the intrinsic properties of exfoliated and CVD grown are, in fact, almost identical. Any spectroscopically observed differences can unambiguously be attributed to the presence or absence of an intercalated water film, respectively. Our findings are further supported with experiments performed on aged samples and extended to a prototypical MoS₂-graphene heterostructure. From our results we conclude that MoS₂ grown with the right precursor (AHM) may serve as a more-than-adequate substitute for exfoliated material.

Results and Discussion

Overview and Key Question We start by introducing the sample systems studied in this paper. Figure 1 (a) presents the seven different single layer MoS₂ systems under investigation: exfoliated MoS₂ on SiO₂ (blue square), MoS₂ grown by CVD with AHM precursor on SiO₂

(light blue triangle) and transferred onto SiO₂ (light blue square), MoS₂ grown by CVD with MoO₃ powder source on SiO₂ (green triangle) and transferred onto SiO₂ (green square), MoS₂ directly grown on transferred CVD graphene (orange triangle), and CVD grown MoS₂ transferred onto transferred CVD graphene (orange square). The images from the optical microscope are all identical in size – the scalebars correspond to 20 μm. This substantiates one of the well-known advantages of CVD over exfoliation as a fabrication method for 2D materials: a significantly larger flake size.

For a first comparison of our sample systems we performed PL and Raman spectroscopy, see Fig. 1 (b)-(d). The obtained PL spectra in Fig. 1 (b) and (c) show the characteristic exciton and trion peaks of MoS₂.¹⁹⁻²¹ The most prominent peak between 1.8 and 1.9 eV corresponds to the A exciton, the peak around 2.0 eV to the B exciton. The A⁻ trion peak can be found as a shoulder of the A exciton peak around 1.8 eV. Apparently, the spectroscopic signature of single layers of MoS₂ prepared differently shows a large variation. Note that, while the variation between sample systems is large, the spectra shown in Fig. 1 are nevertheless typical and thus representative for any given sample system.

Because our analysis is based on a comparison of differently prepared samples we present in Fig. 2 schematic illustrations of our sample systems together with a compilation of our data before discussing the individual samples further below. In Fig. 2 (b) and (c) the PL intensities (total area of all exciton and trion peaks) and the intensity ratio B/(A+A⁻) for the representative PL spectra from Fig. 1 are shown, respectively. All intensities are normalized to the applied laser power and the integration time, thus to the number of incident photons. The ratio B/(A+A⁻) refers to the (area) intensity ratio of the peaks of the A exciton, the B exciton, and the A⁻ trion, respectively. Figure 2 (d) shows the position of the E_{2g}¹ (around 385 cm⁻¹) and the A_{1g} (around 405 cm⁻¹) Raman mode as an average of the acquired Raman spectra. In addition to spectroscopy we performed supportive AFM measurements to determine the thickness of the MoS₂ layers, see SI for a selection of AFM images and line scans and Fig. 2 (e) for the resulting thicknesses. Note that the intercalated

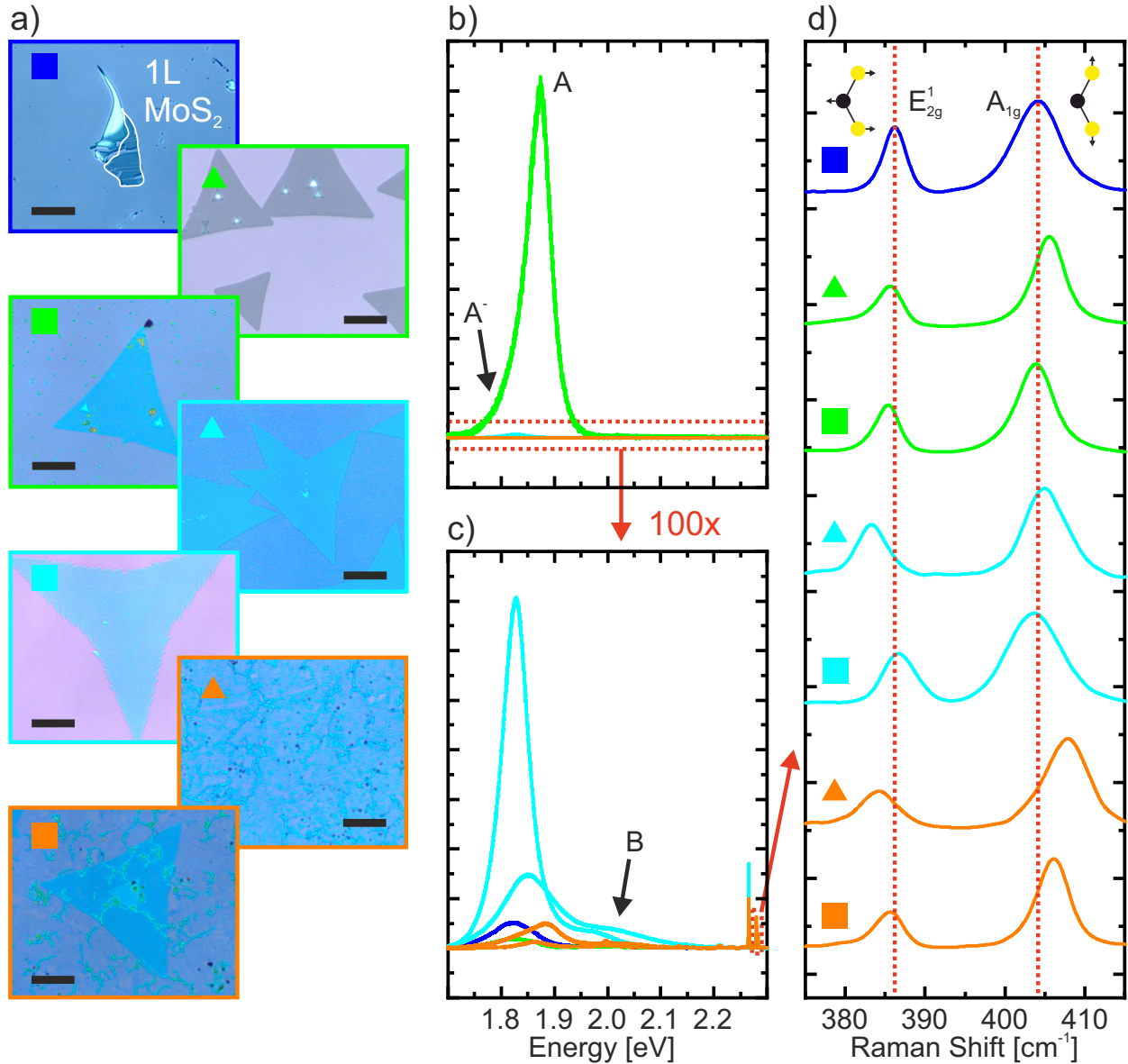


Figure 1: Overview of all sample systems. (a) Images of optical microscopy. The black bar is equivalent to $20\ \mu\text{m}$ in all images. Symbols and colors group the samples. Squares: Exfoliated or transferred MoS_2 . Triangles: MoS_2 grown directly by CVD. Blue: exfoliation. Green: CVD with MoO_3 . Light blue: CVD with AHM. Orange: graphene- MoS_2 heterostructures. (b) and (c) Representative PL spectra of all samples. (d) E_{2g}^1 and A_{1g} mode of all samples. Red line indicates mode positions for exfoliated MoS_2 .

water layers depicted in Fig. 2 (a) were not added on purpose to our sample system. They are nevertheless present and turn out to be the key factor for some of the properties as will be shown further below.

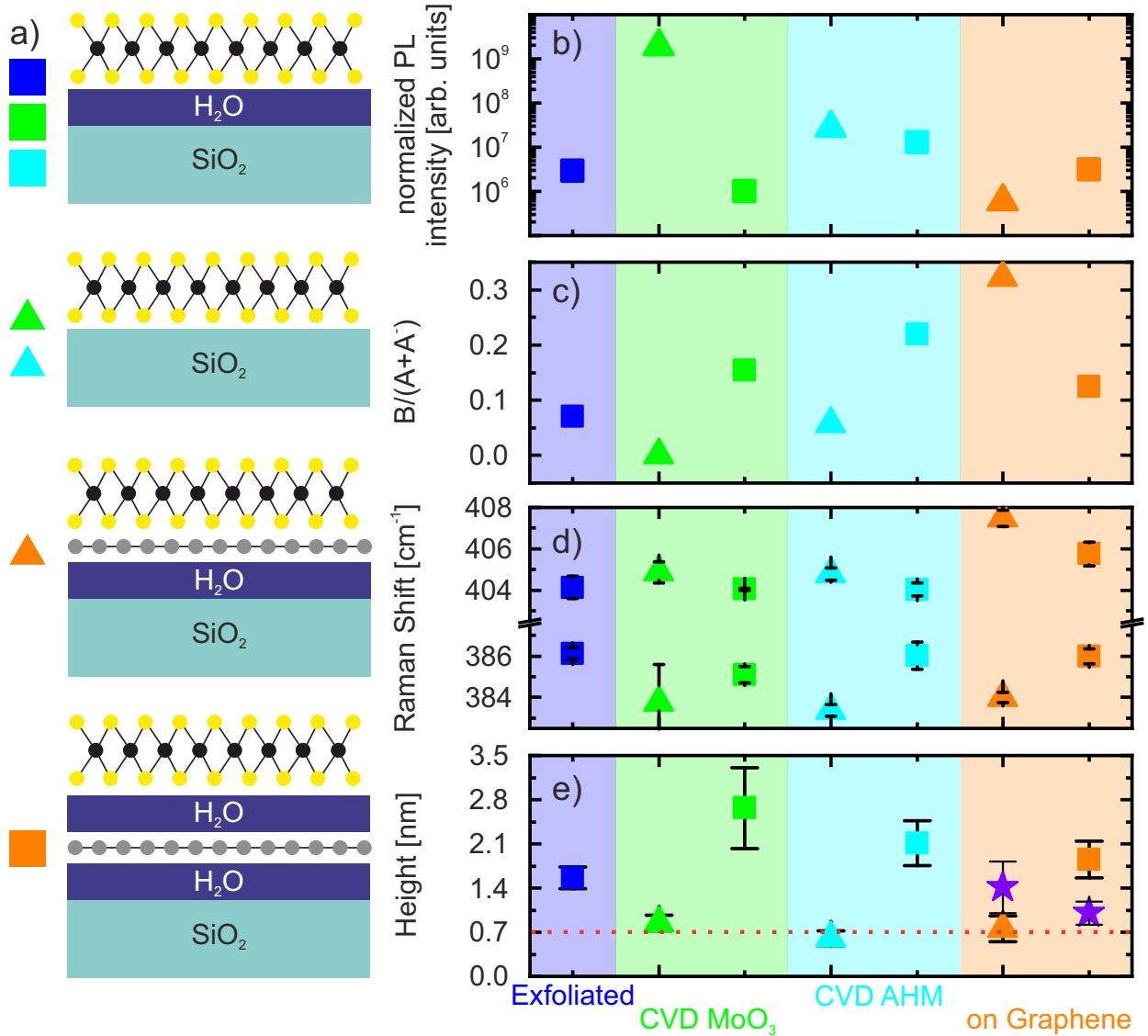


Figure 2: Illustration of the sample systems and compilation of all our data. (a) Schematic illustration of the sample systems with an assignment to the real samples by symbols. (b) PL intensities, (c) $B/(A+A^-)$ exciton peak intensity ratio, (d) Raman mode positions, and (e) MoS₂ (and graphene - purple star) height recorded by AFM for all sample systems.

In order to reveal the origin of the systematic variations we will now discuss the individual features in detail by discussing PL, Raman, and AFM results for each sample system. We start by comparing the two most well known single layer MoS₂ systems: exfoliated (blue squares) and directly grown CVD MoS₂ (green and light blue triangles), both on SiO₂. From Fig. 2 (b) it can be seen that the total PL intensity of CVD grown MoS₂ is up to

three orders of magnitude larger than for the exfoliated counterpart. Therefore, from the PL point of view CVD MoS₂ is clearly superior to exfoliated MoS₂. The higher intensities make CVD MoS₂ the material of choice for optoelectronic applications.

From the PL spectra more information about the MoS₂ can be extracted. Mak et al. reported a decreasing A/A⁻ ratio with increasing charge carrier concentration in single layer MoS₂.²¹ Actually, the A exciton intensity is almost exclusively influenced by the charge carrier concentration. Although not discussed by Mak et al., but shown by their data, the B exciton as well as the A⁻ trion intensity remains relatively constant with changing charge carrier concentration. As it can be difficult to separate the A and the A⁻ peak correctly – they are only a few 10 meV separated from each other – we use the B/(A+A⁻) ratio instead. From this, it can be qualitatively concluded that a high B/(A+A⁻) ratio means that the system is n-doped. For our comparison of CVD grown MoS₂ (green and light blue triangles) with exfoliated MoS₂ (blue square) this means that the latter is more n-doped by charge transfer from the substrate, see Fig. 2 (c). Unfortunately, the exciton peak ratio is not linearly dependent on the carrier concentration and the peaks – both, shifts and intensity ratio change – can be affected due to several other reasons such as defects,^{22,23} strain,^{9,10,12,14,24,25} incident laser power,^{22,25–27} and dielectric screening.^{25,28} Thus, the PL spectra are not suitable for a quantitative analysis, but will be used supportively in the following.

Next, we will show that the commonly used rule for single layer characterization by Raman spectroscopy has to be adapted for CVD material. The typical approach to interpret Raman spectra of MoS₂ is to determine the difference between the position of the E_{2g}¹ and the A_{1g} mode. The result gives an information about the number of layers: for exfoliated MoS₂ a difference of ~19 cm⁻¹ corresponds to single layer, while a difference of ~22 cm⁻¹ is already attributed to a bilayer.²⁹ Here, we find a difference of 18.0 ± 0.75 cm⁻¹ for exfoliated MoS₂ (blue square), 21.1 ± 1.55 cm⁻¹ (green triangle), and 21.4 ± 0.46 cm⁻¹ (light blue triangle) for the MoS₂ grown by the two different CVD methods, see Fig. 2 (d). The latter wave

numbers are already quite close to the number for a bilayer in the case of exfoliated samples. However, the high PL intensity is a clear indication of the single layer nature of the grown material.^{19,20,30} This is further corroborated by the AFM data from Fig. 2 (e). It shows that the determined thickness of the directly grown MoS₂ flakes (triangles) corresponds well with the expected thickness of one layer of MoS₂ (~ 0.7 nm). This is clear evidence, that the CVD MoS₂ is indeed single layer. Exfoliated MoS₂ flakes (blue square) are frequently found to be much thicker, but are identified as single layer from the Raman data. The reason for the increased thickness is most likely due to intercalated water between substrate and 2D material, which is often reported for exfoliated 2D materials.^{2,31-36} In contrast, during the CVD process the presence of a water film appears to be highly unlikely because temperatures up to 800 °C are present. As a result, the grown 2D material is in direct contact with the substrate and its true height might be accessed via AFM. The reason for the unusually large difference between the two Raman peaks in CVD grown MoS₂ is thus not due to the presence of bilayer. Rather, the Raman mode positions are also affected by strain⁷⁻¹⁴ and the charge carrier concentration.^{13,15} The shift of the E_{2g}¹ mode to higher and of the A_{1g} mode to lower values, respectively, indicate qualitatively that the CVD material is exposed to higher strain and exhibits a lower charge carrier concentration. This will be discussed in more detail below.

So far we have seen that exfoliated and CVD grown MoS₂ obviously differ in PL intensity, but also in doping and strain. This leads us to one of the key question of this paper. It is usually assumed that 2D materials grown by CVD directly as single layer have a lower structural quality than exfoliated materials, which are claimed to have a remarkably high quality.^{1,2} The defect density and the grain size will of course affect the material's properties but is this, and therefore the production method, really the reason for the observed differences in the properties of CVD grown MoS₂ and exfoliated MoS₂?

In order to answer this question we prepare sample systems from CVD grown MoS₂ which can be directly compared to exfoliated MoS₂. To this end CVD MoS₂ flakes were transferred

from their original growth substrate SiO_2 onto a second, clean SiO_2 substrate (green and light blue squares). The analysis of this system shows a decreased PL intensity, an increased $B/(A+A^-)$ ratio, a decreased Raman mode difference, and an increased flake thickness, see Fig. 2 (b)-(e). This means, that after the transfer of the CVD grown flake, the properties of the material appear now very similar, even almost identical, to those of exfoliated MoS_2 (for this reason this type of samples is represented by a square in all diagrams, just like exfoliated MoS_2). This finding is even more intriguing as one would have expected the transfer to rather degrade the overall quality of the material. Based on our results, we can at this point thus formulate two hypotheses: (i) the fabrication method itself has only a very minor influence on the intrinsic properties of single layer MoS_2 , and (ii) the dominant factor for the actual properties of 2D MoS_2 is the presence or absence of an intercalated water film - which is a purely external effect.

Quantification by Transformation Matrix Next, we will quantify the physical properties to validate our hypotheses. To this end, we present the Raman mode positions (from Fig. 2) for the differently prepared MoS_2 systems in a different way: In Fig. 3 (a) the E_{2g}^1 mode position is plotted vs. the A_{1g} mode position. This diagram makes it easier to identify groups of sample systems with similar behaviour. For the analysis we construct a matrix T based on literature data taking into account the mode dependency on strain⁷⁻¹⁴ and doping^{13,15} allowing us to conduct an axis transformation as given by equation 1. All publications that have studied the evolution of Raman mode positions as a function of strain report that strain causes a shift of the E_{2g}^1 , while the A_{1g} mode position is almost exclusively influenced by doping. Biaxial¹¹⁻¹³ and uniaxial strain,^{7-10,13,14} however, differ with respect to the exact number of wave number shift per percentage of strain. Although MoS_2 typically deforms in uniaxially strained wrinkles (orders of magnitude larger than the substrate roughness),^{10,37-40} we assume that on the nanoscale the deformation of a MoS_2 layer on a given substrate is a mixture of strained, unstrained, uniaxially and biaxially strained regions averaged by the

μm^2 laser spot. For the construction of the matrix T we use thus the publication of Rice et al.⁷ and Chakraborty et al.,¹⁵ who have quantified the strain- and doping-dependent Raman shift experimentally and by calculations. Note that Rice et al. only report uniaxial strain, which may cause some deviation in the absolute value.

$$\begin{pmatrix} -0.490 \text{ \%/cm}^{-1} & -0.073 \text{ \%/cm}^{-1} \\ 0.088 \times 10^{13} \text{ cm}^{-2}/\text{cm}^{-1} & -0.464 \times 10^{13} \text{ cm}^{-2}/\text{cm}^{-1} \end{pmatrix} \begin{pmatrix} \Delta E_{2g}^1 \\ \Delta A_{1g} \end{pmatrix} = \begin{pmatrix} \Delta Strain \\ \Delta Doping \end{pmatrix} \quad (1)$$

This matrix can now be used to transform our E_{2g}^1 vs. A_{1g} plot (or mode positions of a single spectrum with respect to a given reference spectrum) into a strain vs. n-doping plot, see Fig. 3 (b). Because mode position changes are considered with regard to a reference system, only relative strain and doping are shown. The ideal reference system would be a single layer MoS_2 system with no strain and the intrinsic doping level. Unfortunately, especially the latter has not been achieved yet. For our discussion here we use exfoliated MoS_2 as a reference (i.e. zero point for the axes in Fig. 3 (b)), a choice which can be justified by the following reasons: Exfoliation of single layer MoS_2 is based on the detachment of the last layer from a bulk crystal. Even if the scotch tape would induce any strain in bulk MoS_2 , the multi layered nature of MoS_2 in combination with the weak van der Waals forces in between layers ensure that any strain built into the last layer is released upon exfoliation.

From the resulting diagram (Fig. 3 (b)) the strain and the n-doping can now be quantified with respect to exfoliated MoS_2 . As stated in our hypothesis and shown qualitatively before, transferred CVD grown MoS_2 (green and light blue square) has very similar properties to exfoliated MoS_2 (blue square) indeed. However, directly grown MoS_2 (green and light blue triangle) is more strained by 1–1.5 % and has a reduced electron concentration by approximately $0.55 \times 10^{13} \text{ cm}^{-2}$. Both property changes can be explained by the absence of an intercalated water layer in the case of directly grown MoS_2 and will be discussed separately in the following.

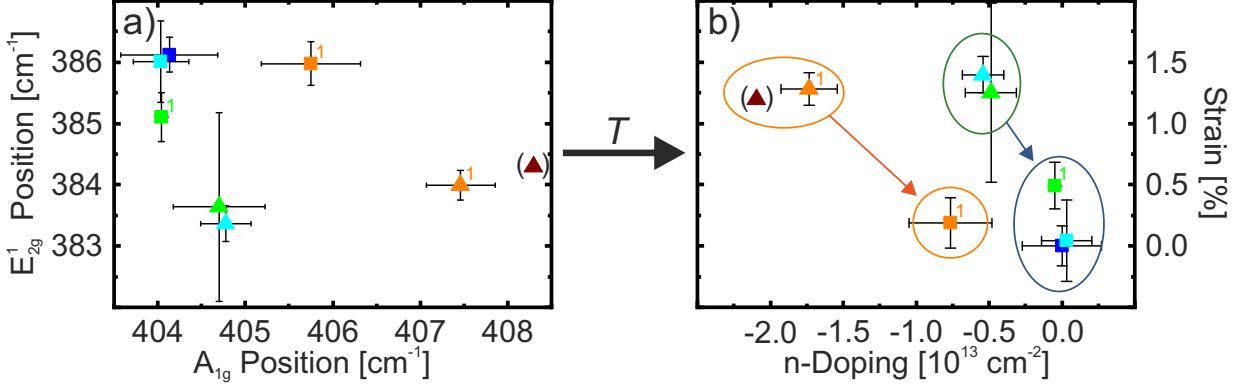


Figure 3: Transformation of the diagram of (a) the measured Raman mode positions to (b) the corresponding physical properties (strain, doping). Groups of sample systems with similar properties become apparent. Brown triangle: MoS₂ grown on highly oriented pyrolytic graphite.⁴¹

Doping Focusing on the x-axis in Fig. 3 (b) we can confirm our hypotheses based on the qualitative analysis (see above) for the property *doping*. First, we find that the intercalated water film between MoS₂ and SiO₂ either acts as a donor or efficiently screens the acceptors of the substrate, i.e., it has an n-doping influence on MoS₂. This is consistent with previous publications which demonstrate by PL that exfoliated MoS₂ on SiO₂ is more n-doped compared to MoS₂ on other substrates⁴² or freestanding MoS₂.¹¹ In case of MoS₂ on mica Varghese et al. showed, that the intercalated water film plays a crucial role for the doping level.³⁶ In addition to comparable PL measurements they performed Kelvin probe microscopy revealing an increased work function of MoS₂ with an intercalated water film in comparison to MoS₂ in direct contact with the substrate.

Even more remarkable is how closely the data points in Fig. 3 (b) match with respect to the average doping level. Transferred CVD MoS₂ (green and light blue square) deviates from exfoliated MoS₂ (blue square) by only 5×10^{11} charge carriers per cm². The electron concentration of MoS₂ samples from the different CVD variants (green and light blue triangle) differ by less than 6×10^{11} cm⁻². This analysis clearly shows that neither the CVD process (defects or impurity atoms) nor the transfer (PMMA residues) causes an effective doping relative to exfoliated MoS₂. As a consequence, we conclude that the various fabrication

methods do not influence the intrinsic carrier concentration in MoS₂.

Strain In the following paragraphs we want to discuss the relative *strain* plotted on the y-axis in Fig. 3 (b). In contrast to directly grown MoS₂ (green and light blue triangle), for exfoliated (blue square) or transferred MoS₂ (green and light blue square), respectively, we find lower strain values. One possible explanation for these findings is related to the properties of the substrate. The arithmetic average roughness $R_a = 0.2$ nm measured on SiO₂ is rather high with respect to the MoS₂ layer thickness (unchanged before and after the MoS₂ growth process – see SI). This may lead to a much stronger bending of 2D material sheets in direct contact with the substrate in comparison to 2D material sheets decoupled from the substrate by an intercalated water film. An illustration of this effect is given in Fig. 4 (b) and (c). Both hypotheses are thus confirmed again, but not as strictly as in the case of doping. This has to do with the comparably large variation of strain values, see the large error bar for the green triangle and the large scatter of the squares in Fig. 3.

The large variation of the strain value is only observed when comparing MoS₂ flakes from different batches grown with the MoO₃ precursor (green triangle), and even if all process parameters are kept constant. However, MoS₂ flakes from the same batch have very similar Raman mode positions and thus strain values, see Tab. 1. The large variation of strain values between batches correlates with the poor reproducibility of this growth variant, which may sometimes not even yield single layer MoS₂, and might be related to the poor control of the exact amount and the relative position of the MoO₃ powder with respect to the substrate. In contrast, the growth process with AHM as precursor (light blue triangle) is in general much more reproducible and always results in single layer MoS₂ flakes with rather constant Raman mode positions when comparing different batches. Obviously, the CVD growth does have an influence on the strain dependent E_{2g}¹ Raman mode of MoS₂.

Another cause that exclusively shifts the E_{2g}¹ mode are sulfur vacancies.⁴³ Because of the very similar change of the Raman signature of MoS₂ it is reasonable that strain and sulfur

Table 1: Raman spectroscopy data from three selected batches of triangular shaped, single layer MoS₂ successfully grown with MoO₃ precursor.

Batch #	E _{2g} ¹ [cm ⁻¹]	A _{1g} [cm ⁻¹]	rel. Strain [%]	rel. n-Doping [10 ¹³ cm ⁻²]
1	385.58 ± 0.39	405.25 ± 0.56	0.35 ± 0.18	-0.57 ± 0.23
2	381.89 ± 0.29	404.48 ± 0.05	2.10 ± 0.10	-0.53 ± 0.04
3	383.47 ± 0.18	404.38 ± 0.25	1.31 ± 0.09	-0.36 ± 0.11
all	383.64 ± 1.54	404.70 ± 0.53	1.25 ± 0.73	-0.49 ± 0.17

vacancies may be related: the missing atoms cause the other lattice atoms to reorient and thus lead to local strain in the lattice. In our previous study we have shown that MoS₂ grown by CVD is indeed MoS_{2-x},⁴⁴ i.e. the major defect type are sulfur vacancies, which has also been reported by another comparative study.⁶ Therefore, it is very likely that the large error bar of the E_{2g}¹ mode, and the corresponding strain value, respectively, are due to varying sulfur vacancy densities in different MoS₂ samples grown with the MoO₃ precursor, i.e. due to different stoichiometries of MoS_{2-x}.

Because different MoS₂ flakes from one batch of the MoO₃ process variant (green triangle) have similar Raman spectra, but can strongly differ from MoS₂ flakes of another batch (Tab. 1), it is thus reasonable that the stoichiometry changes due to, e.g., slightly different (and uncontrollable) source material concentrations during the growth process. In the extreme case the process environment is in a state too far away from a stable stoichiometry of MoS_{2-x}, so that no growth takes place or the resulting MoS_{2-x} immediately degrades again. Otherwise, different sulfur vacancy concentrations are possible, thus different E_{2g}¹ mode positions are found. Because the E_{2g}¹ mode position may not only depend on the strain but also on the defect density, possibly associated with the strain, we can estimate the maximum variation of defect density of both process variants according to the experimental data of Parkin et al.⁴³ We find for MoO₃ precursor based CVD MoS₂ (green triangles) a deviation of sulfur vacancies of about ± 0.79 %, while for MoS₂ from the AHM process (light blue) a value of only ± 0.15 % is determined. It is quite remarkable, that these different defect concentrations do not seem to have any effect on the doping. This is however in agreement with DFT calculations showing that the sulfur defect states are located to deep in the band

gap to cause doping.⁴⁵

Note, that transfer can be used for a reduction of strain, see green and light blue squares in Fig. 3 (b). Our data shows that strain in CVD grown MoS₂ sheets due to a rough SiO₂ substrate is however only partially released when the substrate is removed, see the deviation of the green square (one sample) with respect to the blue and light blue squares and the large error bar of the light blue square in Fig. 3 (b). The polymer – which can introduce additional strain into the MoS₂ by forming bubbles and wrinkles within the polymer layer³⁷ – obviously maintains the in-built strain even if the 2D material is transferred to a new substrate with an intercalated water layer, see schematic in Fig. 4 (c).

In summary, we can basically confirm both hypotheses: we found that the fabrication method has no particular influence on the intrinsic doping level of MoS₂. In contrast, the sulfur vacancy density in CVD MoS₂, which can be monitored by the strain sensitive E_{2g}¹ Raman mode, depends on the growth conditions during the process. Nevertheless, the major factor for the apparent difference between CVD grown and exfoliated MoS₂ is *extrinsic*: intercalated water. The following paragraphs provide further insight into the role of intercalated water and confirms that exfoliated MoS₂ is indeed a good reference because there is only little strain, if any.

Aging We start this additional discussion with some observations from a detailed (although non-comprehensive) aging study (Fig. 4). For this study a CVD grown MoS₂ sample with a low defect density (green triangles), a transferred CVD MoS₂ sample (green squares), and an exfoliated MoS₂ sample (blue squares) were stored for several months under inert nitrogen atmosphere at a humidity of about 20 % to avoid degradation.⁴⁶ We found that particularly the strain in both CVD based systems was reduced to the level of exfoliated MoS₂, while the strain of the exfoliated reference sample remained constant (Fig. 4 (a)). The altered strain in the transferred CVD MoS₂ sample towards the strain level of exfoliated MoS₂ confirms the hypothesis of strain being introduced by the polymer during the transfer.

A possible explanation is illustrated in Fig. 4 (b) and (c): In transferred MoS₂ (Fig. 4 (c)) only in-plane forces are exerted by strain, which let the MoS₂ layer relax on its buffer water layer. In contrast, the net forces in CVD MoS₂ can be more complex because of the rough substrate (Fig. 4 (b)). When the MoS₂ relaxes, channels may form between the MoS₂ layer and the substrate, which would be partially filled up with water from the residual humidity. Two additional observations were made in our aging study: (i) The doping level for all sample systems changes only marginally (Fig. 4 (a)), (ii) the PL intensity only changes significantly for CVD MoS₂ (green triangles), see Fig. 4 (d)-(f), hence with respect to optoelectronic properties this sample system is most sensitive to storage time. Note: Raman and PL spectra were obtained at different locations and on different flakes of the stored samples, but obviously no spatial variations were detected.

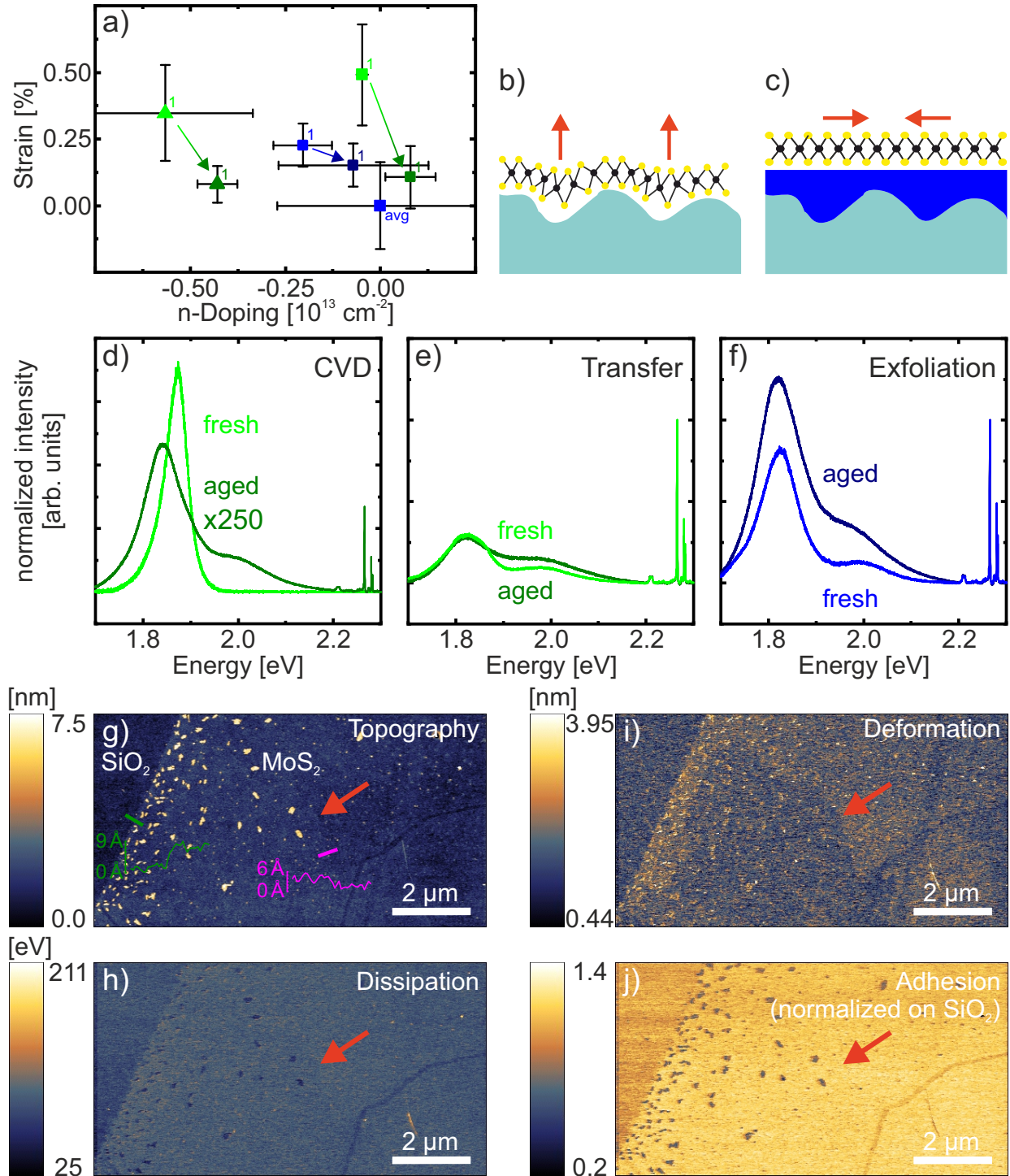


Figure 4: Aging effect of differently prepared MoS₂ samples. (a) Strain and doping values from the Raman mode position before (bright) and after (darker) storage time. Schematic of net forces assumed to be present due to in-plane strain in CVD MoS₂ (b) as grown and (c) subsequently transferred on SiO₂. (d)-(f) PL Peaks before (brighter curves) and after (darker curves) aging. PeakForce AFM channels of an aged, directly CVD grown MoS₂ flake, i.e. (g) topography, (h) dissipation, (i) deformation, (j) adhesion.

Intercalated Water To test the hypothesis of the strain reduction mechanism in aged CVD MoS₂ we performed AFM measurements shown in Fig. 4 (g)-(j). Here we take advantage of the so-called PeakForce Tapping mode, which allows us to additionally obtain nanomechanical properties such as *deformation* (Fig. 4 (i)) and *adhesion* (Fig. 4 (j)). Already when looking at the more common channels *topography* (Fig. 4 (g)) and *dissipation* (Fig. 4 (h)) the effect of aging can be clearly seen (red arrow pointing on the same spot in all images). While some parts of the flake are still found to be 0.7 nm thick (green line profile), most areas show a slight increase in height by 2-4 Å (magenta averaged line profile) and exhibit a reduced dissipation (corresponding to a reduction of inelastic deformation by the AFM tip). The nanomechanical data confirms this further because the deformation of MoS₂ decreases in those areas. The adhesion force between AFM tip and the MoS₂ surface, in contrast, remains constant over the whole sample area. At this point we can exclude the possibility that the contrast changes of the topography, dissipation, and deformation channels are caused by an adsorbate layer on top of the MoS₂ layer because adhesion, which is a measure for the force needed to remove the tip from the surface, remains unchanged. Instead, the slightly higher regions are areas of MoS₂, underneath which a film of intercalated water already exists. The increase in height by a few Angstroms is in good agreement with the characteristic thickness of a single water molecule layer underneath 2D materials, which was determined to be 0.37 nm.^{31,32} The reduced deformation by the AFM tip in this region shows that this water film is incompressible.

For the water intercalation we propose the following mechanism, which is shown step-by-step in Fig. 5. As grown CVD MoS₂ is in direct contact with the rough SiO₂ substrate, causing in-plane strain (Fig. 5 (a)). This results in net forces which partially detach the MoS₂ layer from the SiO₂ substrate and open small channels (Fig. 5 (b)). These channels are subsequently filled with water due to capillary forces (Fig. 5 (c)). It is very likely that this filling even supports the channel formation and thus the strain reduction, i.e., step (b) and (c) take place simultaneously. Over time the intercalated water in the channels expands

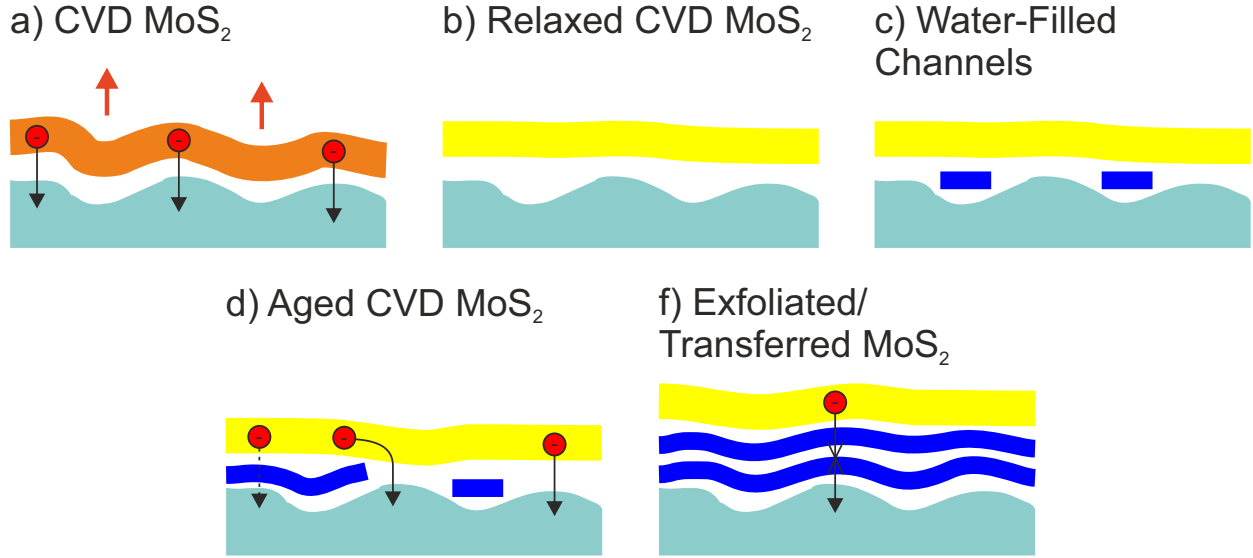


Figure 5: Proposed water intercalation mechanism. (a) Single layer MoS₂ as grown by CVD. In-plane strain (indicated by orange in contrast to the yellow colouring) results in out-of-plane net forces. (b) By relaxing the CVD MoS₂ layer channels between MoS₂ and the substrate are formed. (c) These channels are filled with water due to capillary forces. (d) The water intercalation expands from the water-filled channels forming a water layer. As the water layer is non-continuous and thin charge transfer between MoS₂ layer and substrate is still possible. (e) Underneath exfoliated or transferred MoS₂ two or more water layers are intercalated, thus the charge transfer to the substrate is strongly screened.

to form water layers underneath the MoS₂ (Fig. 5 (d)). The latter stage is observed in the AFM images in Fig. 4 (g)-(j).

If, as with the aged CVD MoS₂ sample (green triangle), the water film is non-continuous and/or very thin, charge transfer between MoS₂ and substrate may be still present (Fig. 5 (d)). However, if the intercalated water film is continuous and thicker, as in the exfoliated or transferred MoS₂-SiO₂ system (> 2 water layers of ~ 0.37 nm each, illustration: Fig. 5 (e), AFM data: Fig. 2 (e)), the charge transfer is more efficiently screened resulting in a different doping level in MoS₂. A strong PL quenching without a change of the doping level is due to the complex mechanisms which influence the excitons in 2D MoS₂. The thin water film, which allows charge transfer between MoS₂ and the substrate, may affect the excitons by, e.g., changing the dielectric environment ($\epsilon_{H_2O} > \epsilon_{SiO_2}$), which increases the dissociation of excitons,²⁵ probably supported by the exciton diffusion length.⁴⁷ Nonetheless, PL intensity

and doping are obviously not always strictly connected.

MoS₂-Graphene Heterostructures Finally, we have prepared MoS₂-graphene heterostructures in order to gain further insight to the screening effect of the intercalated water film underneath transferred single layer MoS₂. The heterostructures have been prepared by two different routes, see Fig. 6. Both routes start with CVD graphene (Fig. 6 (a)), which has been transferred from its growth substrate to SiO₂ by our recently reported polymer-free transfer technique.⁴⁸ Afterwards, MoS₂ is either transferred onto (Fig. 6 (b)) or grown by CVD on the resulting graphene-SiO₂ substrates (Fig. 6 (c) and (d)). In this way, we can compare two different heterostructures: one, where MoS₂ is in direct contact with graphene and the second one, where a water film with a comparable thickness to exfoliated or transferred MoS₂ on SiO₂ is intercalated, see Fig. 2 (a) for illustrations.

The data and resulting properties can be found in Figs 1-3 using orange as color and the same convention for the symbol shape as before, i.e. data points for directly grown MoS₂ on graphene are represented by the orange triangles and MoS₂ transferred on graphene is represented by the orange squares. Note that for both heterostructure types the graphene layer has an increased thickness due to intercalated water (Fig. 2 (e) purple stars), which remains trapped between graphene and SiO₂ despite high temperatures during the MoS₂ growth process. This is not surprising, as other studies have shown that water intercalated underneath graphene remains trapped after annealing even under UHV conditions.^{34,35}

First, we discuss the morphology of the resulting MoS₂-graphene heterostructures. For the transferred heterostructure we obtain large areas (up to a few hundreds of μm^2) of optically perfect heterostructures, see Fig. 6 (b). In the case of directly grown MoS₂, the whole graphene layer has a more bluish color (Fig. 6 (c)), which is due to MoS₂ nanoflakes on the graphene surface as revealed by AFM (Fig. 6 (d)).

These triangular single layer MoS₂ nanoflakes grow in a preferred orientation within a given graphene domain (the boundary is marked by the white dotted line). At the domain

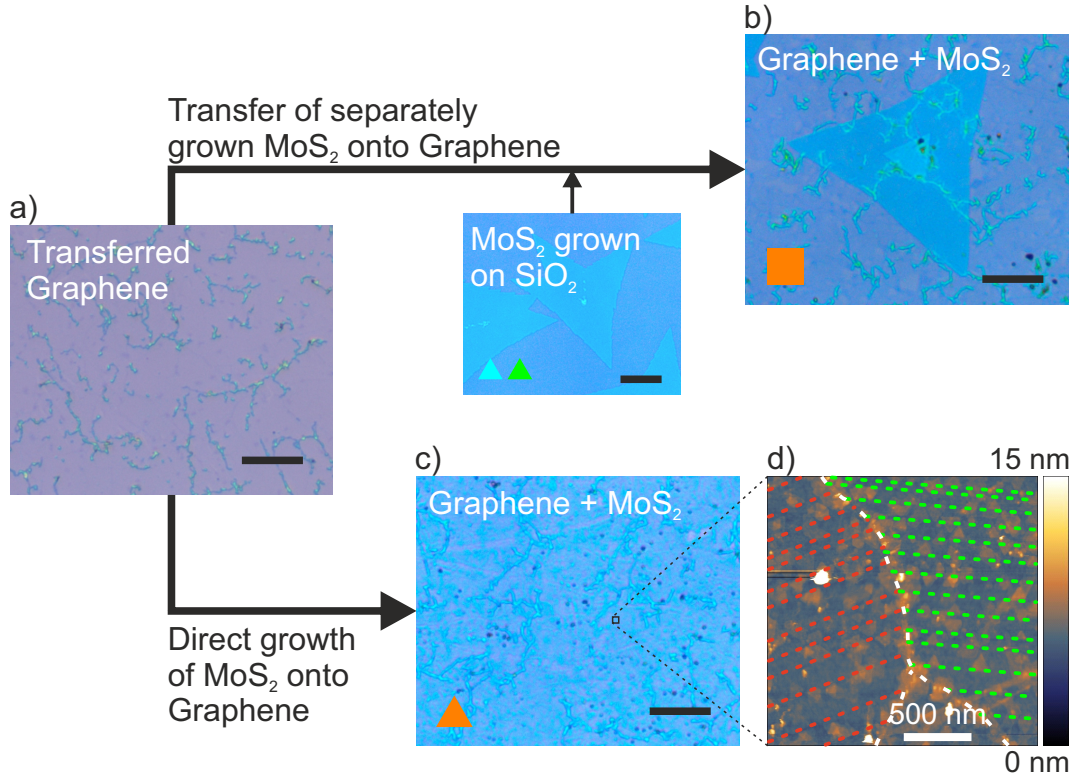


Figure 6: Preparation routes of MoS₂-graphene heterostructures. (a) graphene as transferred onto an SiO₂ substrate as described in our previous study.⁴⁸ (b) Optical image of resulting MoS₂-graphene heterostructure by transferring grown MoS₂ onto graphene. (c) Optical image of MoS₂-graphene heterostructure resulting from direct growth of MoS₂ on graphene. (d) AFM (topography) image of triangular MoS₂ nanoflakes on graphene. Black scale bars correspond to 20 μm .

boundaries a particularly large number of MoS₂ flakes is found. It is typical for MoS₂ to preferentially grow at imperfections such as step edges as demonstrated for “bulk-graphene” highly oriented pyrolytic graphite (HOPG) substrates^{41,49,50} and at artificially induced nm-sized defects.⁵¹ The oriented growth of MoS₂ underlines the cleanliness of the graphene surface after our novel transfer technique.⁴⁸ It is worth noting, that the MoS₂-graphene system based on directly grown MoS₂ (orange triangle) has very similar Raman modes in comparison to MoS₂ grown on HOPG (brown triangles).⁴¹ The similarities of MoS₂ grown on HOPG and on graphene (flake size, nucleation at grain boundaries/step edges, orientation, Raman mode positions) confirm the claim that MoS₂ on HOPG is a good model system for MoS₂ on graphene.^{41,49}

Now let us turn to the spectroscopic results. The trend is very similar to the MoS₂-SiO₂ system, i.e., MoS₂-graphene prepared by transfer (orange squares) is more n-doped and less strained than MoS₂-graphene grown directly (orange triangles), see Fig. 3. However, there is an offset to the corresponding MoS₂-SiO₂ systems. It is not surprising that MoS₂ in direct contact with graphene has a different doping level than MoS₂ in contact with SiO₂ because the electronic structures of graphene and SiO₂ are very different. Because graphene is reported to be p-doped on SiO₂ under ambient conditions,^{1,52} it seems likely that graphene affects the doping level MoS₂ on top towards p-doping. The fact that MoS₂-graphene heterostructure prepared by transfer is less n-doped than MoS₂ transferred on SiO₂ demonstrates that the intercalated water (due to transfer or exfoliation) may not completely screen the substrate. Some charge transfer is still present i.e. the substrate affects the MoS₂ layer despite the intercalated water.

The influence of the substrate (and the role of the intercalated water) can also be seen by the PL intensity of the differently prepared MoS₂-graphene heterostructures (Fig. 2 (b)). MoS₂ transferred onto graphene (orange triangles) exhibits a PL intensity on the same level of MoS₂ transferred or exfoliated onto SiO₂ (green, light blue, blue squares), but is doped more like MoS₂ grown on SiO₂ (green, light blue triangles), see Fig. 3 (b). Obviously the PL intensity of MoS₂ is indeed not strictly related to its doping level, but rather to direct environment of the MoS₂ layer.

This is even more emphasized in the case of MoS₂ directly grown on graphene (orange triangle). Although it is the most p-doped MoS₂ system studied in this paper (Fig. 3 (b)) and should thus have an extremely high PL intensity,²¹ it has the lowest measured PL intensity (Fig. 2 (b)) – even if we take into account that only a fraction of the graphene area is actually covered with single layer MoS₂. In this case, the origin of the PL quenching is the dissociation of the excitons by the underlying semimetallic graphene.⁵³⁻⁵⁵ As previously shown for comparable MoSe₂-graphene heterostructures, the most efficient charge transfer and thus an even stronger PL quenching is to be expected for a direct coupling between the

two van der Waals materials.⁵⁶ Apparently, the direct growth of MoS₂ on graphene via CVD enables such a direct coupling and once more underlines the potential of this fabrication methods also for high quality van der Waals heterostructures.

Conclusion

Exfoliated and CVD grown MoS₂ monolayers appear extremely different – but this is true only at first glance. The CVD material shows a much more intense PL and the mode positions in its Raman spectra differ significantly from those of the exfoliated material. As a consequence, the usual method for evaluating the number of layers, as described by Lee et al.²⁹ and established on exfoliated samples is not valid for MoS₂ grown by CVD. From our spectroscopic results, conclusions can be drawn about different strain and doping values: CVD grown MoS₂ appears to be more strained and less n-doped compared to exfoliated MoS₂. However, the actual origin for the apparent differences in PL and Raman is the presence/absence of an intercalated water film. As soon as a water film is present under the CVD grown MoS₂, the difference in charge carrier density vanishes. Both, the differences in PL intensity and strain/defect density also become much smaller then. The only difference we could identify is a higher/lower density of non-doping defects in the CVD-grown material. Therefore, we draw the clear conclusion from our data that the *intrinsic* properties of MoS₂ grown by CVD and prepared by exfoliation, respectively, are only marginal.

Our data shows that CVD processes run with MoO₃ as precursor typically result in samples with a much larger variation with respect to the strain/defect density values. This indicates the superiority of the AHM precursor for the growth of MoS₂ via CVD and leads us to believe that presumably many other 2D TMDCs may be grown with a similarly high quality if the right precursor can be found.

We could show, that MoS₂ on graphite is indeed a good model system for the investigation of MoS₂-graphene heterostructures. In this case, CVD grown MoS₂ interacts much stronger

with the substrate. A decoupling by an intercalated water film, as typically occurs after exfoliation or transfer, is not sufficient to ensure that the MoS₂ is no longer influenced by the substrate. These findings render heterostructures directly grown via CVD even more promising for energy conversion, sensing, and spintronic devices as one would have expected from proof-of-principle experiments with stacked/transferred van der Waals materials, of which at least one is often exfoliated.^{57–61}

Methods

Sample preparation

The single layer MoS₂ sheets are either prepared by standard exfoliation technique (scotch tape method)^{1,2} (blue squares in the figures) from a natural bulk MoS₂ crystal or by CVD in a three-zone split tube furnace (ThermConcept ROK 70/750/12-3z). Two processes were used: (i) molybdenum trioxide (MoO₃) powder as molybdenum source and referred to as MoO₃ process in the following (green symbols), and (ii) ammonium heptamolybdate (AHM) as precursor for the molybdenum source in the AHM process (light blue symbols). The used recipes follow:

MoO₃ Process This process is a variation of the classical CVD method developed by Lee et al.³ Two heating zones were used here. A ceramic boat with 50 mg sulfur powder (Sigma Aldrich, 99.98 %) is positioned in the upstream heating zone, a ceramic boat with <1 mg MoO₃ powder (Alfa Aesar, 99.95%) and SiO₂ substrates, which are first cleaned in an ultrasonic bath in ethanol and then treated with perylene-3,4,9,10-tetracarboxylic acid tetrapotassium acid salt (PTAS, 2D semiconductors) as the seeding promoter, is positioned in the adjacent downstream heating zone. After an ambient pressure argon flushing of the tube for 30 minutes at an Ar flow of 50 Ncm³/min, which is maintained for the whole process, the heating zone with the MoO₃ powder and the substrates is heated up to a maximum

temperature of 750-800 °C with a rate of 1600 °C/h. With a delay of 30 min the sulfur heating zone is heated to 180 °C within 5 min. After a holding time of 25 min at the maximum temperature, the furnace is opened for rapid cooling.

AHM Process With this process type according to Han et al.,⁵ the molybdenum source, also in the form of MoO₃, is provided in a different way than in the process described above. Instead of adding MoO₃ directly into the process system in powder form, it is first produced from water-soluble ammonium heptamolybdate (AHM, Sigma Aldrich) in an additional decomposition step.^{62,63} Much less than 1 µL (≪ 0.2 mg AHM) is dropleted from a 50:50 mixture of a saturated AHM solution and deionized water onto the previously cleaned substrates and then heated for 30 min at 300 °C to convert AHM to MoO₃. In this way, reproducible and smaller quantities of molybdenum can be introduced into the CVD process system. The seeding promoter cholic acid sodium salt (Sigma Aldrich) is then spun on. After positioning the substrate with the molybdenum source in the downstream heating zone and 50 mg sulfur powder in the upstream heating zone the process can be operated as above. However, for the process slightly different optimal parameters were found: Ar flow is hold at 500 Ncm³/min for the whole process (including at least 15 min flushing time, the process and the cooling time). Both heating zones are heated up within 11 minutes to the process temperatures of 150 °C and 750 °C for the heating zone containing the sulfur source and the heating zone containing the the molybdenum source and the substrates respectively. These process temperatures are held for 19 minutes before the furnace is opened for rapid cooling.

Transfer In order to prepare some of the samples, different transfer techniques are used for the 2D materials MoS₂ and graphene (Graphenea). To transfer MoS₂, a poly(methyl methacrylate) (PMMA) based wet transfer was used. In detail, a thin PMMA layer (ARP 671.05, Allresist GmbH) was spun on the MoS₂ samples and annealed (5 min, 100 °C). In order to remove the PMMA/MoS₂ the SiO₂ is etched by a KOH solution (0.7 mol/L). After replacing the etching solution with deionized water, the floating PMMA/MoS₂ stack

is scooped out by another clean SiO₂ substrate. The PMMA is removed by an acetone bath. For transferring graphene a polymer free wet transfer is used, which is reported in our previous work.⁴⁸ In case of growing MoS₂ onto the graphene-SiO₂ samples, the samples were pre-annealed in activated carbon for 20 min at 100 °C.

Characterization

Confocal Raman and PL spectroscopy were performed with a Raman microscope (Renishaw InVia) with a laser wavelength of 532 nm and a spot size of 1 μm. Power densities of the laser were typically ~0.06 mW/μm², but had to be reduced by several orders of magnitude for samples with extreme PL intensity to avoid saturation of the detector. Atomic force microscope (AFM) measurements were performed on a Veeco Dimension 3100 AFM in Tapping Mode using Nanosensors PPP-NCHR tips and on a Bruker Dimension Icon in PeakForce Tapping Mode with Bruker ScanAsyst-Air tips. The latter mode is based on the recording of a large number of force-distance curves, thus allowing the simultaneous spatial resolution of mechanical properties (deformation, adhesion, ...) in addition to topography.

Acknowledgement

The authors acknowledge support from the German Research Foundation (DFG) by funding SCHL 384/20-1 (project number 406129719). PeakForce AFM, Raman and PL spectroscopy was performed at the Interdisciplinary Center for Analytics on the Nanoscale (ICAN), a core facility funded by the German Research Foundation (DFG, reference RI_00313).

Supporting Information Available

The following files are available free of charge.

The following files are available free of charge.

- Supplementary Material - MoS₂ CVD vs Exfoliation: More AFM images for exemplary MoS₂ thickness and substrate roughness evaluation, additional PeakForce AFM channel

References

- (1) Novoselov, K. S.; Geim, A. K.; Morozov, S. V.; Jiang, D.; Zhang, Y.; Dubonos, S. V.; Grigorieva, I. V.; Frisov, A. A. Electric Field Effect in Atomically Thin Carbon Films. *Science* **2004**, *306*, 666–669.
- (2) Novoselov, K. S.; Jiang, D.; Schedin, F.; Khotkevich, V. V.; Morozov, S. V.; Geim, A. K. Two-Dimensional Atomic Crystals. *Proc. Natl. Acad. Sci. U. S. A.* **2005**, *102*, 10451–10453.
- (3) Lee, Y.-H.; Zhang, X.-Q.; Zhang, W.; Chang, M.-T.; Lin, C.-T.; Chang, K.-D.; Yu, Y.-C.; Wang, J. T.-W.; Chang, C.-S.; Li, L.-J.; Lin, T.-W. Synthesis of Large-Area MoS₂ Atomic Layers with Chemical Vapour Deposition. *Adv. Mater.* **2012**, *24*, 2320–2325.
- (4) Dumcenco, D.; Ovchinnikov, D.; Marinov, K.; Lazić, P.; Gibertini, M.; Marzari, N.; Lopez Sanchez, O.; Kung, Y.-C.; Krasnozhon, D.; Chen, M.-W.; Bertolazzi, S.; Gillet, P.; Fontcuberta i Morral, A.; Radenovic, A.; Kis, A. Large-Area Epitaxial Monolayer MoS₂. *ACS Nano* **2015**, *9*, 4611–4620.
- (5) Han, G. H.; Kybert, N. J.; Naylor, C. H.; Lee, B. S.; Ping, J.; Park, J. H.; Kang, J.; Lee, S. Y.; Lee, Y. H.; Agarwal, R.; Johnson, A. T. C. Seeded Growth of Highly Crystalline Molybdenum Disulphide Monolayers at Controlled Locations. *Nat. Commun.* **2015**, *6*, 6128.
- (6) Hong, J. et al. Exploring Atomic Defects in Molybdenum Disulphide Monolayers. *Nat. Commun.* **2015**, *6*, 6293.

- (7) Rice, C.; Young, R. J.; Zan, R.; Bangert, U.; Wolverson, D.; Georgiou, T.; Jalil, R.; Novoselov, K. S. Raman-Scattering Measurements and First-Principles Calculations of Strain-Induced Phonon Shifts in Monolayer MoS₂. *Phys. Rev. B* **2013**, *87*, 081307.
- (8) Wang, Y.; Cong, C.; Qiu, C.; Yu, T. Raman Spectroscopy Study of Lattice Vibration and Crystallographic Orientation of Monolayer MoS₂ under Uniaxial Strain. *Small* **2013**, *9*, 2857–2861.
- (9) Conley, H. J.; Wang, B.; Ziegler, J. I.; Haglund, R. F.; Pantelides, S. T.; Bolotin, K. I. Bandgap Engineering of Strained Monolayer and Bilayer MoS₂. *Nano Lett.* **2013**, *13*, 3626–3630.
- (10) Castellanos-Gomez, A.; Roldán, R.; Cappelluti, E.; Buscema, M.; Guinea, F.; van der Zant, H. S. J.; Steele, G. A. Local Strain Engineering in Atomically Thin MoS₂. *Nano Lett.* **2013**, *13*, 5361–5366.
- (11) Scheuschner, N.; Ochedowski, O.; Kaulitz, A.-M.; Gillen, R.; Schleberger, M.; Maultzsch, J. Photoluminescence of Freestanding Single- and Few-Layer MoS₂. *Phys. Rev. B* **2014**, *89*, 125406.
- (12) Lloyd, D.; Liu, X.; Christopher, J. W.; Cantley, L.; Wadehra, A.; Kim, B. L.; Goldberg, B. B.; Swan, A. K.; Bunch, J. S. Band Gap Engineering with Ultralarge Biaxial Strains in Suspended Monolayer MoS₂. *Nano Lett.* **2016**, *16*, 5836–5841.
- (13) Kukucska, G.; Koltai, J. Theoretical Investigation of Strain and Doping on the Raman Spectra of Monolayer MoS₂. *Phys. Status Solidi B* **2017**, *254*, 1700184.
- (14) Christopher, J. W.; Vutukuru, M.; Lloyd, D.; Bunch, J. S.; Goldberg, B. B.; Bishop, D. J.; Swan, A. K. Monolayer MoS₂ Strained to 1.3% With a Microelectromechanical System. *J. Microelectromech. Syst.* **2019**, *28*, 254–263.

- (15) Chakraborty, B.; Bera, A.; Muthu, D. V. S.; Bhowmick, S.; Waghmare, U. V.; Sood, A. K. Symmetry-Dependent Phonon Renormalization in Monolayer MoS₂ Transistor. *Phys. Rev. B* **2012**, *85*, 161403.
- (16) Michail, A.; Delikoukos, N.; Parthenios, J.; Galiotis, C.; Papagelis, K. Optical Detection of Strain and Doping Inhomogeneities in Single Layer MoS₂. *Appl. Phys. Lett.* **2016**, *108*, 173102.
- (17) Chae, W. H.; Cain, J. D.; Hanson, E. D.; Murthy, A. A.; Dravid, V. P. Substrate-Induced Strain and Charge Doping in CVD-Grown Monolayer MoS₂. *Appl. Phys. Lett.* **2017**, *111*, 143106.
- (18) Dubey, S. et al. Weakly Trapped, Charged, and Free Excitons in Single-Layer MoS₂ in the Presence of Defects, Strain, and Charged Impurities. *ACS Nano* **2017**, *11*, 11206–11216.
- (19) Mak, K. F.; Lee, C.; Hone, J.; Shan, J.; Heinz, T. F. Atomically Thin MoS₂: A New Direct-Gap Semiconductor. *Phys. Rev. Lett.* **2010**, *105*, 136805.
- (20) Splendiani, A.; Sun, L.; Zhang, Y.; Li, T.; Kim, J.; Chim, C.-Y.; Galli, G.; Wang, F. Emerging Photoluminescence in Monolayer MoS₂. *Nano Lett.* **2010**, *10*, 1271–1275.
- (21) Mak, K. F.; He, K.; Lee, C.; Lee, G. H.; Hone, J.; Heinz, T. F.; Shan, J. Tightly Bound Trions in Monolayer MoS₂. *Nat. Mater.* **2013**, *12*, 207–211.
- (22) Tongay, S.; Suh, J.; Ataca, C.; Fan, W.; Luce, A.; Kang, J. S.; Liu, J.; Ko, C.; Raghunathanan, R.; Zhou, J.; Ogletree, F.; Li, J.; Grossman, J. C.; Wu, J. Defects Activated Photoluminescence in Two-dimensional Semiconductors: Interplay between Bound, Charged, and Free Excitons. *Sci. Rep.* **2013**, *3*, 2657.
- (23) Nan, H.; Wang, Z.; Wang, W.; Liang, Z.; Lu, Y.; Chen, Q.; He, D.; Tan, P.; Miao, F.;

- Wang, X.; Wang, J.; Ni, Z. Strong Photoluminescence Enhancement of MoS₂ through Defect Engineering and Oxygen Bonding. *ACS Nano* **2014**, *8*, 5738–5745.
- (24) Frisenda, R.; Drüppel, M.; Schmidt, R.; Michaelis de Vasconcellos, S.; Perez de Lara, D.; Bratschitsch, R.; Rohlfing, M.; Castellanos-Gomez, A. Biaxial Strain Tuning of the Optical Properties of Single-Layer Transition Metal Dichalcogenides. *npj 2D Mater. Appl.* **2017**, *1*, 10.
- (25) Steinhoff, A.; Florian, M.; Rösner, M.; Schönhoff, G.; Wehling, T. O.; Jahnke, F. Exciton Fission in Monolayer Transition Metal Dichalcogenide Semiconductors. *Nat. Commun.* **2017**, *8*, 1166.
- (26) Kaplan, D.; Gong, Y.; Mills, K.; Swaminathan, V.; Ajayan, P. M.; Shirodkar, S.; Kaxiras, E. Excitation Intensity Dependence of Photoluminescence from Monolayers of MoS₂ and WS₂/MoS₂ Heterostructures. *2D Mater.* **2016**, *3*, 015005.
- (27) Chen, F.; Wang, L.; Wang, T.; Ji, X. Enhanced Local Photoluminescence of a Multilayer MoS₂ Nanodot Stacked on Monolayer MoS₂ Flakes. *Opt. Mater. Express* **2017**, *7*, 1365–1373.
- (28) Lin, Y.; Ling, X.; Yu, L.; Huang, S.; Hsu, A. L.; Lee, Y.-H.; Kong, J.; Dresselhaus, M. S.; Palacios, T. Dielectric Screening of Excitons and Trions in Single-Layer MoS₂. *Nano Lett.* **2014**, *14*, 5569–5576.
- (29) Lee, C.; Yan, H.; Brus, L. E.; Heinz, T. F.; Hone, J.; Ryu, S. Anomalous Lattice Vibrations of Single- and Few-Layer MoS₂. *ACS Nano* **2010**, *4*, 2695–2700.
- (30) Kuc, A.; Zibouche, N.; Heine, T. Influence of Quantum Confinement on the Electronic Structure of the Transition Metal Sulfide TS₂. *Phys. Rev. B* **2011**, *83*, 244059.
- (31) Xu, K.; Peigen, C.; Heath, J. R. Graphene Visualizes the First Water Adlayers on Mica at Ambient Conditions. *Science* **2010**, *329*, 1188–1191.

- (32) Komurasaki, H.; Tsukamoto, T.; Yamazaki, K.; Ogino, T. Layered Structures of Interfacial Water and Their Effects on Raman Spectra in Graphene-on-Sapphire Systems. *J. Phys. Chem. C* **2012**, *116*, 10084–10089.
- (33) Ochedowski, O.; Kleine Bussmann, B.; Ban d’Etat, B.; Lebius, H.; Schleberger, M. Manipulation of the Graphene Surface Potential by Ion Irradiation. *Appl. Phys. Lett.* **2013**, *102*, 153103.
- (34) Ochedowski, O.; Bussmann, B. K.; Schleberger, M. Graphene on Mica - Intercalated Water Trapped for Life. *Sci. Rep.* **2014**, *4*, 6003.
- (35) Temmen, M.; Ochedowski, O.; Schleberger, M.; Reichling, M.; Bollmann, T. R. J. Hydration Layers Trapped between Graphene and a Hydrophilic Substrate. *New J. Phys.* **2014**, *16*, 053039.
- (36) Varghese, J. O.; Agbo, P.; Sutherland, A. M.; Brar, V. W.; Rossman, G. R.; Gray, H. B.; Heath, J. R. The Influence of Water on the Optical Properties of Single-Layer Molybdenum Disulfide. *Adv. Mater.* **2015**, *27*, 2734–2740.
- (37) Lin, Z.; Zhao, Y.; Zhou, C.; Zhong, R.; Wang, X.; Tsang, Y. H.; Chai, Y. Controllable Growth of Large-Size Crystalline MoS₂ and Resist-Free Transfer Assisted with a Cu Thin Film. *Sci. Rep.* **2015**, *5*, 18596.
- (38) Deng, S.; Gao, E.; Xu, Z.; Berry, V. Adhesion Energy of MoS₂ Thin Films on Silicon-Based Substrates Determined via the Attributes of a Single MoS₂ Wrinkle. *ACS Appl. Mater. Interfaces* **2017**, *9*, 7812–7818.
- (39) Pollmann, E.; Madauß, L.; Zeuner, V.; Schleberger, M. Strain in Single-Layer MoS₂ Flakes Grown by Chemical Vapor Deposition. *Wandelt, K., (Ed.) Encyclopedia of Interfacial Chemistry: Surface Science and Electrochemistry* **2018**, 338–343.

- (40) Deng, S.; Che, S.; Debbarma, R.; Berry, V. Strain in a Single Wrinkle on an MoS₂ Flake for In-Plane Realignment of Band Structure for Enhanced Photo-Response. *Nanoscale* **2019**, *11*, 504–511.
- (41) Pollmann, E.; Morbec, J. M.; Madauß, L.; Bröckers, L.; Kratzer, P.; Schleberger, M. Molybdenum Disulphide Nanoflakes Grown by Chemical Vapour Deposition on Graphite: Nucleation, Orientation, and Charge Transfer. *J. Phys. Chem. C* **2020**, *124*, 2689–2697.
- (42) Buscema, M.; Steele, G. A.; van der Zant, H. S. J.; Castellanos-Gomez, A. The Effect of the Substrate on the Raman and Photoluminescence Emission of Single-Layer MoS₂. *Nano Res.* **2014**, *7*, 561–571.
- (43) Parkin, W. M.; Balan, A.; Liang, L.; Das, P. M.; Lamparski, M.; Naylor, C. H.; Rodríguez-Manzo, J. A.; Johnson, A. T. C.; Meunier, V.; Drndić, M. Raman Shifts in Electron-Irradiated Monolayer MoS₂. *ACS Nano* **2016**, *10*, 4134–4142.
- (44) Madauß, L. et al. Highly Active Single-Layer MoS₂ Catalysts Synthesized by Swift Heavy Ion Irradiation. *Nanoscale* **2018**, *10*, 22908–22916.
- (45) Komsa, H.-P.; Krasheninnikov, A. V. Native Defects in Bulk and Monolayer MoS₂ from First Principles. *Phys. Rev. B* **2015**, *91*, 125304.
- (46) Gao, J.; Li, B.; Tan, J.; Chow, P.; Lu, T.-M.; Koratkar, N. Aging of Transition Metal Dichalcogenide Monolayers. *ACS Nano* **2016**, *10*, 2628–2635.
- (47) Wang, R.; Ruzicka, B. A.; Kumar, N.; Bellus, M. Z.; Chiu, H.-Y.; Zhao, H. Ultrafast and Spatially Resolved Studies of Charge Carriers in Atomically Thin Molybdenum Disulfide. *Phys. Rev. B* **2012**, *86*, 045406.
- (48) Madauß, L.; Pollmann, E.; Foller, T.; Schumacher, J.; Hagemann, U.; Heckhoff, T.; Herder, M.; Skopinski, L.; Breuer, L.; Hierzenberger, A.; Wittmar, A.; Lebius, H.;

- Ulbricht, M.; Joshi, R.; Schleberger, M. A Swift Technique to Hydrophobize Graphene and Increase its Mechanical Stability and Charge Carrier Density. *npj 2D Mater. Appl.* accepted.
- (49) Koós, A. A.; Vancsó, P.; Magda, G. Z.; Osváth, Z.; Kertész, K.; Dobrik, G.; Hwang, C.; Tapasztó, L.; Biró, L. P. STM Study of the MoS₂ Flakes Grown on Graphite: A Model System for Atomically Clean 2D Heterostructure Interfaces. *Carbon* **2016**, *105*, 408–415.
- (50) Lu, C.-I.; Butler, C. J.; Huang, J.-K.; Hsing, C.-R.; Yang, H.-H.; Chu, Y.-H.; Luo, C.-H.; Sun, Y.-C.; Hsu, S.-H.; Yang, K.-H. O.; Wei, C.-M.; Li, L.-J.; Lin, M.-T. Graphite Edge Controlled Registration of Monolayer MoS₂ Crystal Orientation. *Appl. Phys. Lett.* **2015**, *106*, 181904.
- (51) Pollmann, E.; Ernst, P.; Madauß, L.; Schleberger, M. Ion-Mediated Growth of Ultra Thin Molybdenum Disulfide Layers on Highly Oriented Pyrolytic Graphite. *Surf. Coat. Technol.* **2018**, *349*, 783–786.
- (52) Ernst, P.; Kozubek, R.; Madauß, L.; Sonntag, J.; Lorke, A.; Schleberger, M. Irradiation of Graphene Field Effect Transistors with Highly Charged Ions. *Nucl. Instrum. Methods Phys. Res. B* **2016**, *382*, 71–75.
- (53) Pierucci, D.; Henck, H.; Naylor, C. H.; Sediri, H.; Lhuillier, E.; Balan, A.; Rault, J. E.; Dappe, Y. J.; Bertran, F.; Le Fèvre, P.; Johnson, A. T. C.; Ouerghi, A. Large Area Molybdenum Disulphide-Epitaxial Graphene Vertical Van der Waals Heterostructures. *Sci. Rep.* **2016**, *6*, 26656.
- (54) Zhang, W.; Chuu, C.-P.; Huang, J.-K.; Chen, C.-H.; Tsai, M.-L.; Chang, Y.-H.; Liang, C.-T.; Chen, Y.-Z.; Chueh, Y.-L.; He, J.-H.; Chou, M.-Y.; Li, L.-J. Ultrahigh-Gain Photodetectors Based on Atomically Thin Graphene-MoS₂ Heterostructures. *Sci. Rep.* **2014**, *4*, 3826.

- (55) Huo, N.; Wei, Z.; Meng, X.; Kang, J.; Wu, F.; Li, S.-S.; Wei, S.-H.; Li, J. Interlayer Coupling and Optoelectronic Properties of Ultrathin Two-Dimensional Heterostructures Based on Graphene, MoS₂ and WS₂. *J. Mater. Chem. C* **2015**, *3*, 5467–5473.
- (56) Froehlicher, G.; Lorchat, E.; Berciaud, S. Charge Versus Energy Transfer in Atomically Thin Graphene-Transition Metal Dichalcogenide van der Waals Heterostructures. *Phys. Rev. X* **2018**, *8*, 011007.
- (57) Dankert, A.; Dash, S. P. Electrical Gate Control of Spin Current in van der Waals Heterostructures at Room Temperature. *Nat. Commun.* **2017**, *8*, 16093.
- (58) Roy, K.; Padmanabhan, M.; Goswami, S.; Sai, T. P.; Kaushal, S.; Ghosh, A. Optically Active Heterostructures of Graphene and Ultrathin MoS₂. *Solid State Commun.* **2013**, *175-176*, 35–42.
- (59) Yu, W. J.; Liu, Y.; Zhou, H.; Yin, A.; Li, Z.; Huang, Y.; Duan, X. Highly Efficient Gate-Tunable Photocurrent Generation in Vertical Heterostructures of Layered Materials. *Nat. Nanotechnol.* **2013**, *8*, 952–958.
- (60) Cho, B.; Yoon, J.; Lim, S. K.; Kim, A. R.; Kim, D.-H.; Park, S.-G.; Kwon, J.-D.; Lee, Y.-J.; Lee, K.-H.; Lee, B. H.; Ko, H. C.; Hahm, M. G. Chemical Sensing of 2D Graphene/MoS₂ Heterostructure Device. *ACS Appl. Mater. Interfaces* **2015**, *7*, 16775–16780.
- (61) Zhao, M.; Song, P.; Teng, J. Electrically and Optically Tunable Responses in Graphene/Transition-Metal-Dichalcogenide Heterostructures. *ACS Appl. Mater. Interfaces* **2018**, *10*, 44102–44108.
- (62) Hanafi, Z. M.; Khilla, M. A.; Askar, M. H. The Thermal Decomposition of Ammonium Heptamolybdate. *Thermochim. Acta* **1981**, *45*, 221–232.

- (63) Wienold, J.; Jentoft, R. E.; Ressler, T. Structural Investigation of the Thermal Decomposition of Ammonium Heptamolybdate by in situ XAFS and XRD. *Eur. J. Inorg. Chem.* **2003**, *6*, 1058–1071.

TOC Graphic

